Sustainability and Durability of Solidia Cement Concrete

Based on alternative CO_2-functional cement chemistry

by Sada Sahu and Richard C. Meininger

Ordinary portland cement (OPC) production is a significant contributor to global greenhouse gas (GHG) emissions. In fact, the cement industry is the second-largest industrial GHG emitter. World cement production reached 4.10×10^9 tonnes (4.5×10^9 tons) in 2019[1] and is estimated to contribute about 8% of total anthropogenic carbon dioxide (CO_2) emissions worldwide.[2]

During the United Nations Framework Convention on Climate Change (UNFCCC) COP 21 meeting in Paris, France, member nations agreed to the goal of keeping the global temperature rise within 2°C (3.6°F) of the preindustrial era level by the end of the twenty-first century (The Paris Agreement).[3] Following the International Energy Agency's guidelines to meet this scenario, the World Business Council for Sustainable Development's Cement Sustainability Initiative group, now part of the Global Cement and Concrete Association, developed a Global Technology Roadmap called "Low-Carbon Transition in the Cement Industry."[4] This roadmap has set a target to reduce the CO_2 emissions from 2.2×10^9 tonnes (2.4×10^9 tons) in 2014 to 1.7×10^9 tonnes (1.9×10^9 tons) by 2050. This goal was set despite a predicted 12 to 23% growth in worldwide cement production during this period. To achieve this goal, a radically new approach to cement manufacturing and use must be undertaken, and an alternative CO_2-functional cement chemistry must be found.

This article describes the CO_2 savings in the production of Solidia Cement™ (SC) and CO_2 use during the production of SC concrete.

Cement and CO_2 Emissions

Portland cement

OPC clinker is produced by burning a mixture of calcareous and siliceous raw materials. Calcareous material (such as limestone) and siliceous materials (such as sand, clay, or similarly composed materials) are ground and sintered at a temperature of about 1450°C (2642°F) in a rotary kiln. The resulting clinker nodules are then ground with about 5% gypsum to produce cement. OPC production emits CO_2 by two direct mechanisms:

- The decomposition of $CaCO_3$ to produce CaO(s) and CO_2(g); and
- Burning of fossil fuels to achieve the sintering temperature in the kiln.

CO_2 emissions are also indirectly created during the mining, transportation, crushing, and grinding of raw materials to create the raw meal feed to the kiln as well as during final grinding of the cement clinker. Many of these processes use electricity. While emissions from electricity generation can vary widely depending on the energy source, emissions associated with electricity comprise only about 10% of the total CO_2 emissions associated with OPC production. Further, CO_2 emissions associated with electricity-powered processes are roughly equivalent for production of either SC or OPC. Therefore, the CO_2 emissions from the use of electricity are omitted in the calculations presented herein.

OPC clinker typically contains up to 70% CaO by weight. The calcination of limestone used to achieve this proportion of CaO releases about 540 kg (1190 lb) of CO_2 gas per tonne (1.1 ton) of clinker.[5] The CO_2 emitted from combustion within the kiln can vary depending on the type and efficiency of the kiln, as well as the type of fuel used. A high-efficiency kiln with a five-stage preheater and precalciner has an efficiency of 58%, which results in a CO_2 emission of about 270 kg (595 lb) per tonne of clinker. An older wet-process kiln with an efficiency of 26% can have a CO_2 emission from combustion as high as 600 kg (1323 lb) per tonne of clinker.[5] The calcination and combustion process of portland clinker production contributes an associated specific CO_2 emission of 810 to 1146 kg (1786 to 2526 lb) per tonne of clinker produced.

Solidia Cement

SC is a new type of binder with a chemistry and functionality that allows it to have a significantly reduced CO_2 footprint. In contrast to the high-lime alite ($3CaO{\cdot}SiO_2$, C_3S), belite ($2CaO{\cdot}SiO_2$, C_2S), tricalcium aluminate ($3CaO{\cdot}Al_2O_3$, C_3A), and tetracalcium aluminoferrite ($4CaO{\cdot}Al_2O_3{\cdot}Fe_2O_3$, C_4AF) phases of OPC, SC comprises low-lime calcium silicate phases such as wollastonite/pseudowollastonite ($CaO{\cdot}SiO_2$, CS) and rankinite ($3CaO{\cdot}2SiO_2$, C_3S_2). Further, SC does not exhibit flash set, so gypsum addition is not required during the grinding process.

Because the lime content of SC is 45 to 70% lower than the lime content of OPC, CO_2 emissions are reduced during the calcination process. Also, because SC clinker is sintered at about 1250°C (2282°F) rather than at 1450°C as required for OPC clinker, the fuel consumption and associated CO_2 emissions are also reduced. The reductions are summarized in Table 1. The details of the CO_2 saving opportunities are also discussed in previous publications,[6,7] and they have been demonstrated during several industrial production trials.[8]

Cement and Concrete Testing

This section describes tests of SC concrete. The SC clinker was produced using limestone and sand typically used for OPC production. These constituents were ground to 82% passing 200 mesh, and the resulting material was processed in an industrial rotary kiln with a four-stage preheater associated with a precalciner. The burning zone temperature was maintained at about 1250°C. The produced clinker was ground using a vertical roller mill (VRM) to a Blaine fineness of about 500 m^2/kg and particle size d_{50} of 12 to 14 µm determined by laser diffraction in water suspension using Mastersizer 2000 software.

Table 1:
Summary of CO_2 emissions for OPC and SC clinker

	CO_2 emission		
Source	Per tonne of OPC clinker, kg	Per tonne of SC clinker, kg	Reduction, %
Calcination	540	375	30
Combustion	270	190	30
Total CO_2 emission	810	565	30

Note: 1 kg = 2.2 lb;1 tonne = 1.1 ton

Table 2:
Mixture proportions of air-entrained SC concrete

Ingredients	Quantity, kg/m^3
SC	350.0
Concrete sand (FM = 2.35)	821.0
Coarse aggregate 3/8 in. (9.5 mm)	414.0
Coarse aggregate 3/4 in. (19 mm)	737.0
Water	136.0
High-range water-reducing admixture	5 mL/kg of cement
Air-entraining admixture	3 mL/kg of cement
Set-retarding admixture	5 mL/kg of cement

Note: 1 kg/m^3 = 1.7 lb/yd^3; 1 mL/kg = 0.015 fl oz/lb

Chemical and phase analyses

The SC clinker was sampled and analyzed for elemental composition by X-ray fluorescence (XRF) and phase composition by X-ray diffraction (XRD). Clinker samples were made into fused glass beads for XRF analysis and measured using a Panalytical Axios WDS spectrometer. XRD data was collected using a Panalytical Cubix^3 diffractometer with 1600W Cu K_α radiation from 5° to 65° 2Θ, 0.017°/s, 60s per step. Amorphous content was determined by comparison of the collected pattern to a crystalline rutile standard. The reported silica was the sum of quartz, cristobalite, and tridymite.

Concrete and mortar formulation and curing

Air-entrained concrete with 3/4 in. (19 mm) maximum size coarse aggregate was produced using the mixture proportions provided in Table 2. The water-cement ratio (*w*/*c*) was maintained at 0.39. Concrete cylinders measuring 100 x 200 mm (4 x 8 in.) and prisms measuring 75 x 100 x 400 mm (3 x 4 x 15-3/4 in.), 100 x 100 x 350 mm (4 x 4 x 14 in.), and 150 x 150 x 525 mm (6 x 6 x 21 in.) were cast. The concrete samples were demolded after curing in ambient conditions for about 6 hours and further cured in a 100% CO_2 environment for 72 hours at elevated temperatures (<100°C [212°F]).

The cured samples were tested for compressive strength according to ASTM C39/C39M, "Standard Test Method for Compressive Strength of Cylindrical Concrete Specimens"; tensile strength according to ASTM C496/C496M, "Standard Test Method for Splitting Tensile Strength of Cylindrical Concrete Specimens"; flexural strength according to ASTM C78/C78M, "Standard Test Method for Flexural Strength of Concrete (Using Simple Beam with Third-Point Loading)"; and elastic modulus according to ASTM C469/C469M, "Standard Test Method for Static Modulus of Elasticity and Poisson's Ratio of Concrete in Compression." Freezing-and-thawing resistance tests were carried out on prisms measuring 75 x 100 x 400 mm, according to Procedure A of ASTM C666/C666M, "Standard Test Method for Resistance of Concrete to Rapid Freezing and Thawing."

Mortar bars measuring 25 x 25 x 300 mm (1 x 1 x 12 in.) with ASTM C490/C490M gauge studs for length change measurement were prepared following the procedure described in ASTM C227, "Standard Test Method for Potential Alkali Reactivity of Cement-Aggregate Combinations (Mortar-Bar Method) (Withdrawn 2018)," for alkali-silica reaction (ASR) testing. The mixture proportions

for the mortar are provided in Table 3. These mortar mixtures were produced using the same admixtures as concrete mixtures but without the air-entraining admixture. To comply with the gradation requirement, a small percentage of the concrete sand was used in addition to the reactive fused silica sand. The reference OPC used in the study had a total alkali content Na_2Oeq of 0.96%. The mortar bars were precured in the mold for about 5 hours before demolding. The demolded SC mortar bars were further cured in a 100% CO_2 atmosphere for 40 hours. The alkali-aggregate reaction tests were carried out according to the test procedure described in ASTM C227. The length change measurements were made weekly for the first 4 weeks and subsequently every 4 weeks.

Mortar bars measuring 25 x 25 x 300 mm with ASTM C490/C490M gauge studs for length change measurement were also prepared following the procedure described in ASTM C1012/C1012M, "Standard Test Method for Length Change of Hydraulic-Cement Mortars Exposed to a Sulfate Solution." The mixture proportions for the mortar are provided in Table 4. Mortar mixtures included a high-range water-reducing admixture dosed by mass (weight) of cement (3 mL/kg [0.05 fl oz]). The mortar bars were precured in the mold for about 5 hours before demolding. The demolded SC mortar bars were further cured in a 100% CO_2 atmosphere for 40 hours. The test specimens were exposed to 352 moles of sodium sulfate solution (50 g/L). Sulfate expansion tests were carried out according to the test procedure described in ASTM C1012/C1012M. The length change measurements were made weekly for the first 4 weeks and subsequently every 4 weeks.

Table 3:
Mixture proportions of mortar for ASR testing

Ingredients	Quantity, g
SC or OPC	600
Fused silica sand	1317
Concrete sand	333
Water	175
High-range water-reducing admixture	5 mL/kg of cement
Set-retarding admixture	5 mL/kg of cement

Note: 1 g = 0.035 oz; 1 mL/kg = 0.015 fl oz/lb

Table 4:
Mixture proportions of mortar for sulfate-resistance testing

Ingredients	Quantity, g
SC or OPC	500
ASTM standard sand	1375
Water	175
High-range water-reducing admixture	3 mL/kg of cement

Note: 1 g = 0.035 oz; 1 mL/kg = 0.015 fl oz/lb

Air-void analysis

Air-void content and distribution in hardened concrete were measured by an automated air-void analyzer, RapidAir457. This procedure is consistent with Procedure C in ASTM C457/C457M, "Standard Test Method for Microscopical Determination of Parameters of the Air-Void System in Hardened Concrete."

Scanning electron microscopy (SEM)

A small cut portion of a concrete cylinder was dried, epoxy impregnated, and cured. After curing, one of the surfaces was polished to 1/4-micron finish. The polished surface was sputter coated with carbon and examined under an SEM in backscattered mode at 20 keV.

Results and Discussion

Chemical and phase analysis

The average elemental composition of the SC clinker measured by XRF and expressed as oxides in wt.% was: 46.6 of CaO, 47.9 of SiO_2, 2.6 of Al_2O_3, 0.8 of Fe_2O_3, 0.8 of MgO, 0.4 of Na_2O, 0.7 of K_2O, and 0.2 of SO_3.

The average phase composition of the SC clinker as determined by quantitative XRD with Rietveld refinement is shown in Table 5.

The determined statistics of the particle size distribution were d_{10} of 1.52 µm, d_{50} of 14.56 µm, and d_{90} of 44.30 µm.

Carbonation reactions during curing

The calcium silicate phases present in the SC react with CO_2 as described in Eq. (1) to (3):

$$CaSiO_3(s) + CO_2(g) \xrightarrow{H_2O} CaCO_3(s) + SiO_2(s) \quad (1)$$

$$Ca_3Si_2O_7(s) + 3CO_2(g) \xrightarrow{H_2O} 3CaCO_3(s) + 2SiO_2(s) \quad (2)$$

$$Ca_2SiO_4(s) + CO_2(g) \xrightarrow{H_2O} 2CaCO_3(s) + SiO_2(s) \quad (3)$$

Additionally, the amorphous component of the cement can carbonate to some extent depending on its calcium content

Table 5:
The average phase composition of SC clinker as measured by XRD

Phases	Formula	Concentration, wt. %
Pseudowollastonite	$CaSiO_3$	51.0
Wollastonite	$CaSiO_3$	0.2
Rankinite	$Ca_3Si_2O_7$	13.1
Belite	Ca_2SiO_4	2.7
Amorphous	—	24.4
Melilite	$(Ca,Na,K)_2(Al,Mg,Fe^{2+})[(Al,Si)SiO_7]$	5.9
Brownmillerite	$Ca_2(Fe,Al)_2O_5$	0.6
Silica	SiO_2	1.9
Lime	CaO	0.4

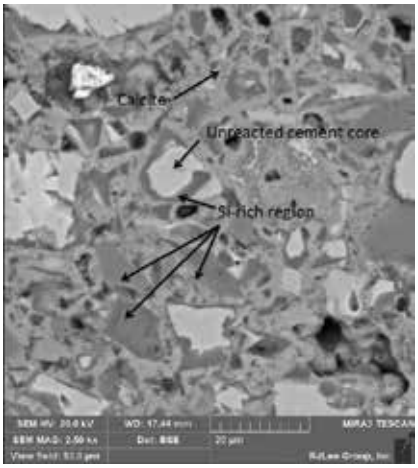

Fig. 1: Field emission scanning electron microscope-backscattered electron (FESEM-BSE) image showing the microstructure of the carbonated paste area of SC concrete

Table 6:
Air-void parameters of SC concrete as determined by ASTM C457/C457M, Procedure C, with four replicates, each starting from a different corner of the prepared polished concrete specimen

TFHRC* ID	Corner	Air content, %	Specific surface, in.$^{-1}$	Spacing factor, in.	Void freq. (void/in.), in.$^{-1}$	Average void length, in.
15219	Corner 1	7.04	660.6	0.0056	11.63	0.0061
	Corner 2	6.9	663.4	0.0057	11.45	0.006
	Corner 3	6.24	619.9	0.0067	9.67	0.0065
	Corner 4	5.91	848.8	0.0051	12.54	0.0047
	Average	6.52	698.18	0.0058	11.32	0.0058

*Turner-Fairbank Highway Research Center

Note: 1 in. = 25 mm

and bulk chemistry. The formation of $CaCO_3$(s) and SiO_2(s) is associated with a net solid volume increase (due to the incorporation of CO_2). This reaction is what gives SC concrete the ability to generate strength, similarly to the solid volume increase produced by hydration in OPC (due to the incorporation of water). Details of the carbonation process of this cement are provided in other publications.[9]

Field emission scanning electron microscopic (FESEM) images of the paste portion of a hardened SC concrete collected in backscattered electron (BSE) imaging mode are provided in Fig. 1. High brightness reactive-phase particles are generally surrounded by a dark rim of calcium-depleted amorphous silica. The space between cement particles is filled with $CaCO_3$ particles of intermediate brightness. The dark area is the porosity left after the carbonation process. The carbonation of SC produces a densified material through the direct precipitation of $CaCO_3$ in the pores, where it acts to bind together the components of the concrete.

Mechanical properties

The mechanical properties of SC concrete determined during testing were:

- Compressive strength of 9150 psi (63 MPa);
- Split tensile strength of 930 psi (6.4 MPa);
- Flexural strength of 780 psi (5.4 MPa);
- Modulus of elasticity of 7,192,000 psi (49,590 MPa); and
- Poisson's ratio of 0.17.

The results show that the performance of the SC concrete produced in this study is comparable to that of OPC concrete of a similar mixture design.

Freezing-and-thawing resistance

While freezing-and-thawing durability is influenced by aggregate type, water content, and mixture composition, air-void content and distribution are dominant factors. As summarized in Table 6, the air-void content and spacing factor determined for the tested SC concrete mixtures are within the ranges considered to provide good protection against cyclic freezing-and-thawing damage.

Assessment of SC concrete freezing-and-thawing durability was performed as specified in Procedure A (freezing in water and thawing in water) of ASTM C666/C666M. This method evaluates the concrete as a function of percentage relative dynamic modulus of elasticity (RDME) with relation to the number of freezing-and-thawing cycles. The results are plotted in Fig. 2(a).

ASTM C666/C666M requires testing up to 300 cycles. Concrete specimens fail the test if the RDME values drop below 60%. As there was not a significant drop in RDME values after 300 cycles, the test was continued until 540 cycles. After 540 cycles, the RDME values remained at 96%. The mass change over this period is plotted in Fig. 2(b), showing that the specimens gained a small amount of mass over the testing period. This is most likely due to saturation of the nanopores present in the silica gel over time.[10] The specimens showed very minor scaling at the end of testing. These results demonstrate that SC concrete has good freezing-and-thawing durability when the appropriate amount and distribution of entrained air voids are present in the system.

ASR resistance

Expansion and cracking, leading to loss of strength, elasticity, and durability, can result from chemical reactions involving hydroxyl ions and alkali ions in OPC (or from other sources) with certain siliceous constituents of aggregates in OPC concrete. The types of silica that are susceptible to ASR are quartz with sufficiently strained or microcrystalline,

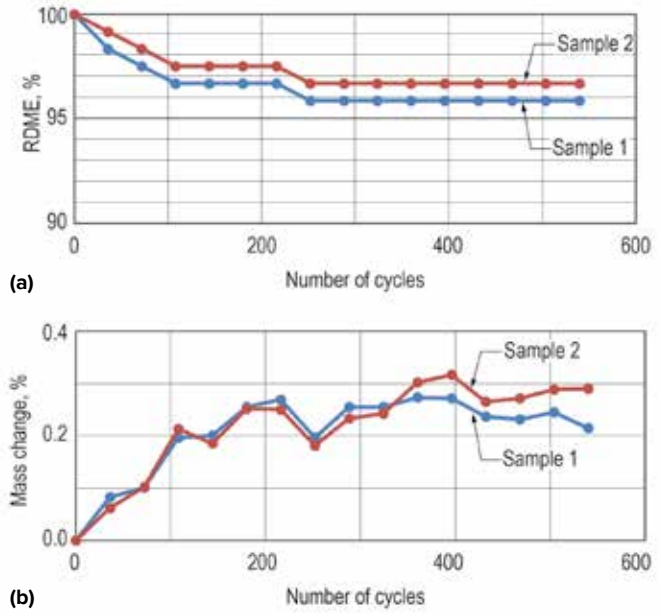

Fig. 2: Freezing-and-thawing testing of SC concrete: (a) relative dynamic modulus of elasticity (RDME); and (b) mass change

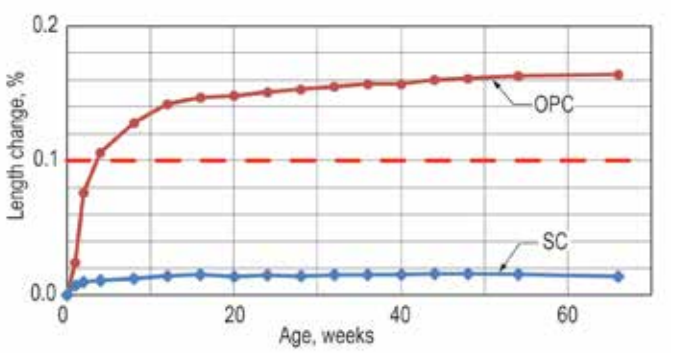

Fig. 3: Length change of mortar bars tested per ASTM C227 for SC and OPC mixtures

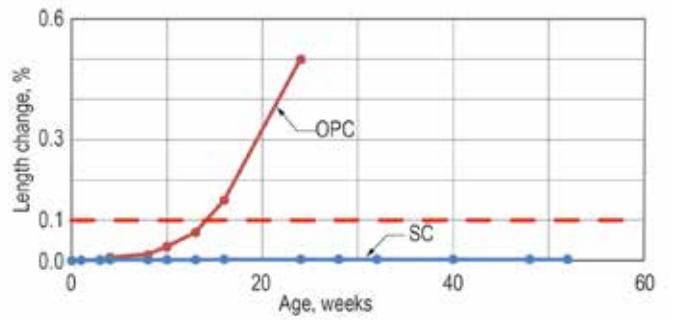

Fig. 4: Length change of OPC and SC mortar bars during exposure to sodium sulfate solution

tridymite, cristobalite, and glass, which can occur in various rock formations such as opals, flints, cherts, and others.[11] This can render the aggregates unusable or potentially detrimental to the performance of OPC concrete. Therefore, ASR resistance in the presence of reactive aggregates is an important factor in concrete durability.

To evaluate the ASR resistance of SC concrete, highly reactive fused silica sand was used in this study. Results of length change measurements of ASTM C227 mortar bars with time are provided in Fig. 3. The results show OPC mortar samples expanded beyond the threshold limit of 0.1% within the first 3 weeks. After about 12 weeks, the expansion rate was significantly reduced. The SC mortar samples showed slight expansion in the initial 2 weeks but did not expand further for the duration of testing.

These results show improved ASR resistance of SC concrete in comparison to the OPC concrete used in this study. Therefore, some of the reactive aggregates that are not usable in OPC concrete could potentially be used in SC concrete.

Sulfate resistance

Upon exposure to sulfate-bearing soil or water, the paste of OPC concrete interacts with sulfate ions to form gypsum and ettringite, leading to expansion and cracking within hardened concrete. Recent studies have also reported formation of thaumasite in colder regions. Thaumasite can cause severe damage to concrete through deterioration of C-S-H, the primary binding phase within the cement paste. As a result, hydraulic cements, especially those high in C_3A content, are susceptible to structural cracking, loss of strength, stiffness reduction, or disintegration in the presence of sulfates.[12,13]

Sulfate resistance of SC mortar was evaluated by measuring the length change of mortar bars exposed to sodium sulfate solution. Results of length change with time are provided in Fig. 4. In this test, OPC mortar samples expanded beyond the threshold limit of 0.1% within the first 16 weeks of exposure and continued to expand significantly. After about 24 weeks, the mortar bars expanded by 0.5% and bowed. No further measurements were obtained for OPC mortar bars, as accurate expansion measurements were unattainable. In contrast, the SC mortar bars showed negligible expansion throughout the testing period.

In comparison to the reference OPC specimen, the SC mortar specimen exhibited significantly improved sulfate resistance, indicating that concrete made with SC may be suitable for use in aggressive sulfate environments.

Conclusions

The production of SC typically results in 30% reductions in CO_2 emission and energy consumption compared to the production of OPC. Concretes using SC also consume up to 300 kg of CO_2 per tonne of SC during CO_2 curing. The carbonation of SC produces calcite ($CaCO_3$) and amorphous silica (SiO_2).

The mechanical properties of SC concrete are equivalent or better than OPC concrete, and they are achieved within a shorter curing period.

SC concrete passes freezing-and-thawing testing in fresh water per ASTM C666/C666M, Procedure A, with RDME greater than 90% after 540 freezing-and-thawing cycles. Also, SC concrete exhibits negligible mass loss due to scaling during the freezing-and-thawing testing.

SC mortar bars exhibit excellent resistance to ASR, as mixtures comprising fused silica sand show minimum expansion. SC mortar bars also exhibit excellent resistance to sulfate attack, as specimens exposed to sodium sulfate solution show minimum expansion.

Acknowledgments

Part of this work was performed under a cooperative agreement between Solidia Technologies and the Federal Highway Administration (FHWA)—DTFH6115H00020. Prior to this agreement, preliminary evaluations were conducted at the FHWA Turner-Fairbank Highway Research Center under a Cooperative Research and Development Agreement (CRADA). FHWA neither endorses nor approves this product and the FHWA name and logo are not to be used in the marketing of the product. The purpose of the cooperative agreements was to evaluate this new proprietary technology with respect to potential applications in highway construction and repair.

References

1. "Mineral Commodity Summaries 2020," U.S. Geological Survey, 2020, p. 43, www.usgs.gov/centers/nmic/mineral-commodity-summaries.

2. Timperly, J., "Q&A: Why Cement Emissions Matter for Climate Change," CarbonBrief, Sept. 13, 2018, www.carbonbrief.org/qa-why-cement-emissions-matter-for-climate-change.

3. "The Paris Agreement," United Nations Framework Convention on Climate Change, www.unfccc.int/process-and-meetings/the-paris-agreement/the-paris-agreement. Accessed Apr. 22, 2020.

4. "Technology Roadmap: Low-Carbon Transition in the Cement Industry," International Energy Agency, Paris, France, 2018, 61 pp., www.wbcsd.org/Sector-Projects/Cement-Sustainability-Initiative/Resources/Technology-Roadmap-Low-Carbon-Transition-in-the-Cement-Industry.

5. Barcelo, L.; Kline, J.; Walenta, G.; and Gartner, E.M., "Cement and Carbon Emissions," *Materials and Structures*, V. 47, No. 6, June 2014, pp. 1055-1065.

6. DeCristofaro, N., and Sahu, S., "CO_2 Reducing Cement," *World Cement*, Jan. 2014, www.worldcement.com/the-americas/09012014/co2_reducing_cement_part_one_solidia_cement_chemistry_and_synthesis_571/.

7. Atakan, V.; Sahu, S.; Quinn, S.; Hu, X.; and DeCristofaro, N., "Why CO_2 Matters—Advances in a New Class of Cement," *ZKG International*, V. 67, No. 3, Jan. 2014, pp. 60-63.

8. DeCristofaro, N.; Meyer, V.; Sahu, S.; Bryant, J.; and Moro, F., "Environmental Impact of Carbonated Calcium Silicate Cement-Based Concrete," *Proceedings of the 1st International Conference on Construction Materials for Sustainable Future*, A. Baricevic, ed., Zadar, Croatia, Apr. 19-21, 2017, pp. 65-70.

9. Sahu, S.; Quinn, S.; Atakan, V.; DeCristofaro, N.; and Walenta, G., "CO_2-Reducing Cement Based on Calcium Silicate," 14th International Congress on the Chemistry of Cement (ICCC), Beijing, China, Oct. 13-16, 2015.

10. Villani, C.; Spragg, R.; Tokpatayeva, R.; Olek, J.; and Weiss, W.J., "Characterizing the Pore Structure of Carbonated Natural Wollastonite," *Proceedings of the 4th International Conference on the Durability of Concrete Structures (ICDCS)*, West Lafayette, IN, July 24-26, 2014, pp. 262-269.

11. Diamond, S., "A Review of Alkali-Silica Reaction and Expansion Mechanisms 1. Alkalies in Cements and in Concrete Pore Solutions," *Cement and Concrete Research*, V. 5, No. 4, July 1975, pp. 329-345.

12. Müllauer, W.; Beddoe, R.E.; and Heinz, D., "Sulfate Attack Expansion Mechanisms," *Cement and Concrete Research*, V. 52, Oct. 2013, pp. 208-215.

13. Tian, B., and Cohen, M.D., "Does Gypsum Formation during Sulfate Attack on Concrete Lead to Expansion?," *Cement and Concrete Research*, V. 30, No. 1, Jan. 2000, pp. 117-123.

Note: Additional information on the ASTM standards discussed in this article can be found at **www.astm.org**.

Selected for reader interest by the editors.

Sada Sahu is a Principal Scientist at Solidia Technologies, Inc., Piscataway, NJ, responsible for the development of Solidia Cement and admixtures compatible with it. His career spans over three decades in the cement and concrete industry in a variety of roles in the production of cement and research, including the development of sulfoaluminate belite cement, radioactive waste immobilization in cementitious grouts, failure analysis of concrete, microstructure development of concrete, development of mineral and organic admixtures for concrete. Sahu came to Solidia from BASF Construction Chemicals. He received his PhD in materials science and engineering from Slovak Technical University, Bratislava, Slovakia, and he has over 60 publications and 10 patents.

Richard C. Meininger, FACI, is a civil engineering pavement and materials Researcher at the Federal Highway Administration (FHWA), Turner-Fairbank Highway Research Center, McLean, VA, principally involved in concrete and aggregates research. He has been at FHWA for more than 15 years and is a licensed professional engineer in Maryland. Meininger has been a member of ACI for 50 years. He is a member of ACI Committees 211, Proportioning Concrete Mixtures; 221, Aggregates; 242, Alternative Cements; and 555, Concrete with Recycled Materials. He is also active on TRB and ASTM International committees. Meininger received degrees in civil engineering and engineering materials from the University of Maryland.